Sensitivity Analysis of Network Parameters With Electromagnetic Frequency-Domain Simulators

Natalia K. Nikolova, *Senior Member, IEEE*, Jiang Zhu, Dongying Li, Mohamed H. Bakr, *Member, IEEE*, and John W. Bandler, *Fellow, IEEE*

***Abstract*—A new practical approach to sensitivity analysis of the network parameters of high-frequency structures with commercial full-wave electromagnetic (EM) solvers is proposed. We show that the computation of the linear-network parameter derivatives in the design-parameter space does not require an adjoint-problem solution. The sensitivities are computed outside the EM solver, which simplifies the implementation. We discuss: 1) features of commercial EM solvers which allow the user to compute network parameters and their sensitivities through a single full-wave simulation; 2) the accuracy of the computed derivatives; and 3) the overhead of the sensitivity computation. Through examples based on FEMLAB and FEKO simulations, comparisons are made with the forward finite-difference derivative estimates in terms of accuracy and CPU time.**

***Index Terms*—Adjoint-variable methods, design automation, frequency-domain analysis, sensitivity analysis.**

I. Introduction

THE importance of the design sensitivity analysis of distributed systems stems from the need to improve their performance or to know their uncertainties [1]. The design sensitivity comprises the response derivatives with respect to shape or material parameters. Manufacturing and yield tolerances, design of experiments and models, and design optimization are aspects of the overall design, which can benefit greatly from the availability of the response sensitivity.

The adjoint-variable method is known to be the most efficient approach to design sensitivity analysis for problems of high complexity where the number of state variables is much greater than the number of the required response derivatives [1]–[3]. General adjoint-based methodologies have been available for some time in control theory [1], and techniques complementary to the finite-element method (FEM) have been developed in structural [2], [3] and electrical [4]–[9] engineering. However, feasible implementations remain a challenge. The reason lies mainly in the complexity of these techniques.

Manuscript received June 16, 2005; revised October 24, 2005. This work was supported in part by the Natural Sciences and Engineering Research Council of Canada under Grant STPGP 269760 and Grant 227660-03.

N. K. Nikolova, J. Zhu, D. Li, and M. H. Bakr are with the Computational Electromagnetics Research Laboratory, Department of Electrical and Computer Engineering, McMaster University, Hamilton, ON, Canada L8S 4K1 (e-mail: talia@mcmaster.ca; zhuj7@univmail.cis.mcmaster.ca; lid6@univmail.cis.mcmaster.ca; mbakr@mail.ece.mcmaster.ca).

J. W. Bandler is with the Simulation Optimization Systems Research Laboratory, Department of Electrical and Computer Engineering, McMaster University, Hamilton, ON, Canada L8S 4K1 and also with Bandler Corporation, Dundas, ON, Canada L9H 5E7 (e-mail: bandler@mcmaster.ca).

Digital Object Identifier 10.1109/TMTT.2005.862663

Recently, a simpler and more versatile approach has been adopted [10]–[13] for analyses with the method of moments (MoM) and the frequency-domain transmission-line method. The effort to formulate analytically the system matrix derivative—which is an essential component of the sensitivity formula—was abandoned as impractical for a general-purpose sensitivity solver. Instead, approximations of the system-matrix derivatives are employed using either finite differences [10] or discrete step-wise changes [12], [13] as dictated by the nature of the discretization grid. Neither the accuracy nor the computational speed is sacrificed.

All of the above approaches require the analysis of an adjoint problem whose excitation is response-dependent. Not only does this mean one additional full-wave simulation, but it also requires modification of the electromagnetic (EM) analysis engine due to the specifics of the adjoint-problem excitation. Notably, Akel and Webb [6] have pointed out that, in the case of the FEM with tetrahedral edge elements, the sensitivity of the S-matrix can be derived without an adjoint simulation.

Here, we formulate a general self-adjoint approach to the sensitivity analysis of network parameters. It requires neither an adjoint problem nor analytical system matrix derivatives. We focus on the linear problem in the frequency domain, which is at the core of a number of commercial high-frequency simulators.[1] Thus, for the first time, we suggest practical and fast sensitivity solutions realized entirely outside the framework of the EM solver. These standalone algorithms can be incorporated in an automated design to perform optimization, modeling, or tolerance analysis of high-frequency structures with any commercial solver, which exports the system matrix and the solution vector.

In Section II, we state the adjoint-based sensitivity formula and the definition of a self-adjoint problem. In Sections III and IV, we introduce the self-adjoint formulas for network-parameter sensitivity calculations. In Section V, we outline the features of the commercial EM solvers, which enable independent network-parameter sensitivity analysis. Numerical validation and comparisons are presented in Section VI. Section VII discusses the computational overhead associated with the sensitivity analysis. We give recommendations for further reduction of the computational cost whenever software changes are possible, and conclude with a summary.

[1]The network-parameter sensitivities with time-domain solvers deserve separate treatment and will be considered elsewhere.

II. Background

A. Sensitivities of Linear Complex Systems

A time-harmonic EM problem involving linear materials can be cast in a linear system of complex equations by the use of a variety of numerical techniques[2]

$$\boldsymbol{A}\boldsymbol{x} = \boldsymbol{b}. \tag{1}$$

The system matrix $\boldsymbol{A} \in \mathbb{C}^{M\times M}$ is a function of the shape and material parameters, some of which comprise the vector of designable parameters $\boldsymbol{p} \in \mathbb{R}^{N\times 1}$, i.e., $\boldsymbol{A}(\boldsymbol{p})$. Thus, the vector of state variables $\boldsymbol{x} \in \mathbb{C}^{M\times 1}$ is a function of $\boldsymbol{p}, \boldsymbol{x}(\boldsymbol{p})$. The right-hand side $\boldsymbol{b}$ results from the EM excitation and/or the inhomogeneous boundary conditions. Typically, in a problem of finding the sensitivities of network parameters, $\boldsymbol{b}$ is independent of $\boldsymbol{p}$, because the waveguide structures launching the incident waves (the ports) serve as a reference and are not a subject to design changes: $\nabla_{\boldsymbol{p}}\boldsymbol{b} = \boldsymbol{0}$.[3]

For the purposes of optimization, the system performance is evaluated through a scalar real-valued objective function $F(\boldsymbol{x}, \boldsymbol{p})$. In tolerance analysis or model generation, we may consider a set of responses, some of which are complex. We first consider a single, possibly complex, function F, and we refer to it as the *response*. It is computed from the solution $\bar{\boldsymbol{x}}$ of (1) for a given design.

Through $\boldsymbol{x}$, F is an implicit function of $\boldsymbol{p}$. It may also have an explicit dependence on $\boldsymbol{p}$. Explicit dependence on a shape parameter p_i ($\partial^e F/\partial p_i \neq 0$) arises when F depends on the field/current solution at points whose coordinates in space are affected by a change in p_i. An example is the explicit dependence of an antenna gain on the position/shape of the wires [10] carrying the radiating currents. Explicit dependence with respect to a material parameter arises when F depends on the field/current solution at points whose constitutive parameters are affected by its change. An example is the stored energy in a volume of changing permittivity. The network parameters, however, are computed from the solution at the ports, whose shape and materials do not change. Thus, when F is a network parameter, $\nabla^e_{\boldsymbol{p}} F = \boldsymbol{0}$.

The derivatives of a complex response $F = F_R + jF_I$ ($j = \sqrt{-1}$) with respect to the design parameters $\boldsymbol{p} = [p_1 \cdots p_N]^T$ can be efficiently calculated using the adjoint-variable sensitivity formula [9], [13]

$$\frac{\partial F}{\partial p_i} = \frac{\partial^e F}{\partial p_i} + \hat{\boldsymbol{x}}^T \cdot \left(\frac{\partial \boldsymbol{b}}{\partial p_i} - \frac{\partial \boldsymbol{A}}{\partial p_i}\cdot \bar{\boldsymbol{x}}\right), \qquad i = 1, 2, \ldots, N. \tag{2}$$

In a compact gradient notation, (2) becomes

$$\nabla_{\boldsymbol{p}} F = \nabla^e_{\boldsymbol{p}} F + \hat{\boldsymbol{x}}^T \cdot \nabla_{\boldsymbol{p}}(\boldsymbol{b} - \boldsymbol{A}\bar{\boldsymbol{x}}). \tag{3}$$

We refer to $\nabla_{\boldsymbol{p}} F$ as the *response sensitivity*. The adjoint-variable vector $\hat{\boldsymbol{x}}$ is the solution to

$$\boldsymbol{A}^T \cdot \hat{\boldsymbol{x}} = (\nabla_{\boldsymbol{x}} F)^T_{\boldsymbol{x}=\bar{\boldsymbol{x}}} \tag{4}$$

where $\nabla_{\boldsymbol{x}} F$ is a row of the derivatives of F with respect to the state variables $x_i, i = 1, \ldots, M$, evaluated at the current solution $\boldsymbol{x} = \bar{\boldsymbol{x}}$. In the case of complex systems, it involves the real $\boldsymbol{x}_R$ and the imaginary $\boldsymbol{x}_I$ parts of the state variables.

As detailed in [13], the complex-response analysis (2)–(4) is valid if F is an analytic function of the state variables $\boldsymbol{x}$, in which case, the Cauchy–Riemann conditions [14] are fulfilled. A convenient form of the adjoint excitation $\hat{\boldsymbol{b}} = (\nabla_{\boldsymbol{x}} F)^T$ is

$$\begin{aligned}\hat{\boldsymbol{b}} &= \left[\left(\frac{\partial F_R}{\partial x_{1_R}} + j\frac{\partial F_I}{\partial x_{1_R}}\right)\cdots\left(\frac{\partial F_R}{\partial x_{M_R}} + j\frac{\partial F_I}{\partial x_{M_R}}\right)\right]^T \\ &= (\nabla_{\boldsymbol{x}_R} F)^T.\end{aligned} \tag{5}$$

B. Sensitivity Expression for Linear-Network Parameters

For a network parameter sensitivity, the gradients $\nabla_{\boldsymbol{p}}\boldsymbol{b}$ and $\nabla^e_{\boldsymbol{p}} F$ vanish, which reduces (3) to

$$\nabla_{\boldsymbol{p}} F = -\hat{\boldsymbol{x}}^T \cdot \nabla_{\boldsymbol{p}}(\boldsymbol{A}\bar{\boldsymbol{x}}). \tag{6}$$

We emphasize that, in (6), $\bar{\boldsymbol{x}}$ is fixed, and only $\boldsymbol{A}$ is differentiated, as in (2).

The sensitivity formula (6) uses three quantities: the solution $\bar{\boldsymbol{x}}$ of the original problem (1), the set of system matrix derivatives $\partial\boldsymbol{A}/\partial p_i, i = 1, \ldots, N$, and the solution $\hat{\boldsymbol{x}}$ to the adjoint problem (4). The first one is available from the EM simulation. Also, we assume that the system matrix derivatives have been already computed, e.g., using finite differences [10] or Broyden's update [15], [16]. We next show that, in the case of the network parameters, the adjoint solution $\hat{\boldsymbol{x}}$ is equal to $\bar{\boldsymbol{x}}$ multiplied by a complex factor κ. Thus, the solution of (4) is unnecessary. We employ the above adjoint-variable theory to determine κ for different network parameters. For that, we also need to know the dependence of the particular network parameter on the distributed field/current solution. We delineate this dependence below.

III. Self-Adjoint S-Parameter Sensitivities

The S-parameters are extracted differently depending on whether the numerical solution is in terms of field vectors (e.g., FEM) or current distributions (e.g., MoM).

A. S-Parameter Sensitivities With Field Solutions

To obtain the full scattering matrix of a K-port structure for a particular mode υ, K solutions of (1) are carried out with one of the ports being excited while the rest of the ports are matched. We assume that the jth port is excited and define the S_{kj} parameters as

$$\begin{aligned} S^{(\upsilon)}_{kj} &= \frac{\iint\limits_{k\text{-port}} (\mathbf{a}_n \times \mathbf{E}^{(\upsilon)}_j)\cdot(\mathbf{a}_n \times \mathbf{e}^{(\upsilon)}_k) ds_k}{\iint\limits_{j\text{-port}} (\mathbf{a}_n \times \mathbf{E}^{(\upsilon)\text{inc}}_j)\cdot(\mathbf{a}_n \times \mathbf{e}^{(\upsilon)}_j) ds_j} - \delta_{kj} \\ \delta_{kj} &= \begin{cases} 1, & k = j \\ 0, & k \neq j \end{cases}. \end{aligned} \tag{7}$$

[2]All matrices are in bold italics (one-dimensional matrices are lowercase, matrices of higher dimensions are uppercase). Vectors in space, e.g., field vectors, are bold uppercase.

[3]We define the gradient operator as a row operator [1], [3], e.g., for a scalar function f, $\nabla_{\boldsymbol{p}} f = [\partial f/\partial p_1 \cdots \partial f/\partial p_N]$. In the case of a column $\boldsymbol{f}$, $\nabla_{\boldsymbol{p}}\boldsymbol{f}$ is a matrix whose rows are the gradients of the respective elements of $\boldsymbol{f}$.

Here,[4] $\mathbf{E}_j^{(\upsilon)\text{inc}}$ is the incident field of the υ mode at the jth port, $\mathbf{E}_j^{(\upsilon)}$ is the resulting $\mathbf{E}$-field solution, $\mathbf{a}_n$ is the unit normal to the respective port surface, and $\mathbf{e}_\xi^{(\upsilon)}, \xi = j, k$, are the normalized real vectors representing the υ-mode $\mathbf{E}$-field distribution across the respective ports. The modal vectors $\mathbf{e}_\xi^{(\upsilon)}$ form an orthonormal basis

$$\iint\limits_{\xi\text{-port}} \left(\mathbf{e}_\xi^{(\upsilon)} \cdot \mathbf{e}_\xi^{(\upsilon')}\right) ds_\xi = \delta_{\upsilon\upsilon'} \tag{8}$$

where $\delta_{\upsilon\upsilon'} = 1$ if the modes υ and υ' are the same, and $\delta_{\upsilon\upsilon'} = 0$ otherwise. They are obtained either analytically or numerically [17], [18]. The analytical expressions for the modes $\mathbf{e}^{(\upsilon)}$ of a rectangular waveguide can be found in [17].

Our formulation (7) uses the approach in [17] where the output power wave in the kth port is obtained by projecting the transverse components of the transmitted/reflected $\mathbf{E}$-field onto the transverse components of the port modal vector $\mathbf{e}_k^{(\upsilon)}$. In the denominator, the input power wave in the jth port is obtained in the same manner. For a single-mode analysis, the typical incident field setup is $\mathbf{E}_j^{(\upsilon)\text{inc}} = E_{0j}\mathbf{e}_j^{(\upsilon)}$ where E_{0j} is a user-defined magnitude. Usually, $E_{0j} = 1$. We note that an alternative formulation, see, e.g., [18], uses the orthonormal set (8) as well as its dual ($\mathbf{H}$-field) vector set. Both S-parameter definitions lead to the same final sensitivity result. We choose to work with (7).

Since we consider the S-parameter sensitivities of a single mode, for simpler notations, the superscript υ is omitted but implied in all formulas hereafter. Thus, with the jth port being excited, the respective right-hand side of (1) is denoted by $\boldsymbol{b}_j$, and its respective solution vector is $\boldsymbol{x}_j$. It represents the field solution $\mathbf{E}_j$. K such solutions $\bar{\boldsymbol{x}}_j, j = 1, \ldots, K$, are available from the S-parameter analysis of the structure.

In the FEM, within each surface element s at a port, the field $\mathbf{E}^s$ is approximated via the $\mathbf{E}$-field components $x_i^s, i = 1, \ldots, n_s$, tangential to the n_s edges of the element [17]

$$\mathbf{a}_n^s \times \mathbf{E}^s = \sum_{i=1}^{n^s} \mathbf{B}_i^s x_i^s = (\boldsymbol{x}^s)^T \cdot \{\mathbf{B}^s\} = \{\mathbf{B}^s\}^T \cdot \boldsymbol{x}^s. \tag{9}$$

Here, $\mathbf{a}_n^s$ is the unit normal to the surface element, $\boldsymbol{x}^s = [x_1^s \cdots x_{n_s}^s]^T$, and $\mathbf{B}_i^s$ are the vector basis functions of the element. The column $\{\mathbf{B}^s\}$ has the $\mathbf{B}_i^s$ vectors as its elements, $\{\mathbf{B}^s\} = [\mathbf{B}_1^s \cdots \mathbf{B}_{n_s}^s]^T$. Note that the vector of edge field components $\boldsymbol{x}^s$ is a subset of the solution $\boldsymbol{x}$ of (1).

If S_{kj} is the response whose sensitivities we need, i.e., $F = S_{kj}$, we must consider the solution of the adjoint problem (4) where the respective adjoint excitation becomes $\hat{\boldsymbol{b}}_{kj} = [\nabla_{\boldsymbol{x}} S_{kj}]^T$. Instead of dealing with the global adjoint excitation vector $[\nabla_{\boldsymbol{x}} S_{kj}]^T$, we can consider its elemental subset $[\nabla_{\boldsymbol{x}^s} S_{kj}]^T$.

[4]If the S-parameters are computed at planes different from their respective ports, deembedding is applied. It is in the form of an additional exponential factor, e.g., for the reflection coefficient, it is $e^{2\gamma L_d}$ where γ is the waveguide propagation constant and L_d is the distance between the port and the plane of deembedding. Also, if the ports have different impedances, a factor of $\sqrt{Z_j/Z_k}$ multiplying (7) must be included. These factors are parameter-independent and do not change the derivations which follow. They are omitted for brevity.

From (7), we see that S_{kj} is a linear and, therefore, analytic function of the field solution $\mathbf{E}_j$, as well as of $\boldsymbol{x}$, as implied by the linear relation (9). Then, the analysis with (4) and (6) applies. We first write (7) in terms of the field of the surface elements of the kth port as

$$S_{kj} = \frac{\sum_{s_k} \int\limits_{s_k\text{-element}} \int (\mathbf{a}_n^{s_k} \times \mathbf{E}_j^s) \cdot (\mathbf{a}_n^{s_k} \times \mathbf{e}_k) ds_{s_k}}{\iint\limits_{j\text{-port}} (\mathbf{a}_n \times \mathbf{E}_j^{\text{inc}}) \cdot (\mathbf{a}_n \times \mathbf{e}_j) ds_j} - \delta_{kj} \tag{10}$$

where δ_{kj} has been already defined in (7). Making use of (9), we have

$$S_{kj} = \frac{\sum_{s_k} \int\limits_{s_k\text{-element}} \int (\{\mathbf{B}^{s_k}\}^T \cdot \boldsymbol{x}^{s_k}) \cdot (\mathbf{a}_n^{s_k} \times \mathbf{e}_k) ds_{s_k}}{\iint\limits_{j-\text{port}} (\mathbf{a}_n \times \mathbf{E}_j^{\text{inc}}) \cdot (\mathbf{a}_n \times \mathbf{e}_j) ds_j} - \delta_{kj}. \tag{11}$$

From (11), we find the derivatives of S_{kj} with respect to the edge field components of the s_k element at the kth port

$$\frac{\partial S_{kj}}{\partial x_i^{s_k}} = \frac{\int\limits_{s_k\text{-element}} \int \mathbf{B}_i^{s_k} \cdot (\mathbf{a}_n^{s_k} \times \mathbf{e}_k) ds_{s_k}}{\iint\limits_{j\text{-port}} (\mathbf{a}_n \times \mathbf{E}_j^{\text{inc}}) \cdot (\mathbf{a}_n \times \mathbf{e}_j) ds_j}, \quad i = 1, \ldots, n_{s_k} \tag{12}$$

where n_{s_k} is the number of edges of the s_k element. In gradient notation, (12) becomes

$$[\nabla_{\boldsymbol{x}^{s_k}} S_{kj}]^T = \frac{\int\limits_{s_k\text{-element}} \int \{\mathbf{B}^{s_k}\} \cdot (\mathbf{a}_n^{s_k} \times \mathbf{e}_k) ds_{s_k}}{\iint\limits_{j\text{-port}} (\mathbf{a}_n \times \mathbf{E}_j^{\text{inc}}) \cdot (\mathbf{a}_n \times \mathbf{e}_j) ds_j}. \tag{13}$$

After the assembly of the FEM equations, each of the elements of $[\nabla_{\boldsymbol{x}^{s_k}} S_{kj}]^T$ becomes an element of the global adjoint excitation vector $\hat{\boldsymbol{b}}_{kj} = [\nabla_{\boldsymbol{x}} S_{kj}]^T$.

We now compare the elements of the adjoint excitation (13) with the elements of the excitation for the s_k element of the kth port in the original FEM problem [17]

$$\boldsymbol{b}^{s_k} = \int\limits_{s_k\text{-element}} \int \{\mathbf{B}^{s_k}\} \cdot (\mathbf{U}_k^{\text{inc}} \times \mathbf{a}_n^{s_k}) ds_{s_k} \tag{14}$$

where

$$\mathbf{U}_k^{\text{inc}} = -2\gamma_k E_{0k} \mathbf{e}_k \tag{15}$$

for a single-mode incident field. Here, $\mathbf{e}_k$ is the normalized modal vector, E_{0k} is a user-defined magnitude (usually set as 1), and γ_k is the modal propagation constant of the port. The comparison reveals a simple linear relationship between the original and adjoint excitation vectors, $\boldsymbol{b}_k$ and $\hat{\boldsymbol{b}}_{kj}$, given as follows:

$$\hat{\boldsymbol{b}}_{kj} = \frac{1}{2\gamma_k E_0 \iint\limits_{j\text{-port}} (\mathbf{a}_n \times \mathbf{E}_j^{\text{inc}}) \cdot (\mathbf{a}_n \times \mathbf{e}_j) ds_j} \cdot \boldsymbol{b}_k. \tag{16}$$

Both $\boldsymbol{b}_k$ and $\hat{\boldsymbol{b}}_{kj}$ are obtained from their respective elemental excitations, $\boldsymbol{b}^{s_k}$ and $[\nabla_{\boldsymbol{x}^{s_k}} S_{kj}]^T$, through identical system-assembly procedures.

Next, we turn to the adjoint solutions $\hat{\boldsymbol{x}}_{kj}$ resulting from $\hat{\boldsymbol{b}}_{kj},\ k,j=1,\ldots,K$. We note that the FEM system matrix $\boldsymbol{A}$ is symmetric (see, e.g., [17]),

$$\boldsymbol{A}=\boldsymbol{A}^T. \tag{17}$$

From (16) and (17), we conclude that all adjoint solutions $\hat{\boldsymbol{x}}_{kj}$ needed for the S -parameter sensitivities can be calculated from the K original solution vectors $\boldsymbol{x}_k, k=1,\ldots,K$, by a simple multiplication with a known complex constant

$$\begin{aligned}\hat{\boldsymbol{x}}_{kj}&=\kappa_{kj}\cdot\boldsymbol{x}_k,\kappa_{kj}\\&=\frac{1}{2\gamma_k E_0\iint\limits_{j\text{-port}}(\mathbf{a}_n\times\mathbf{E}_j^{\text{inc}})\cdot(\mathbf{a}_n\times\mathbf{e}_j)ds_j}.\end{aligned} \tag{18}$$

They are then substituted into (6) where F can be any of the elements of the S-matrix.

The self-adjoint nature of the solution derived above shows that the information necessary to compute the S-parameter sensitivities is already contained in the full-wave solution provided by the FEM simulator. The sensitivity analysis is thus reduced to a relatively simple and entirely independent post-process, which does not require additional full-wave solutions.

B. S-Parameter Sensitivities With Current Solutions

Similarly to the case of the field solution considered above, the S-parameters depend on the current density solutions produced by the MoM solvers through simple linear relations. More specifically, the current solution at the ports is needed.

Consider the calculation of the S-parameters of a network of system impedance Z_0 by FEKO [19]

$$S_{kj}=\delta_{kj}-\frac{2Z_0 I_{k,j}}{V_j^e},\qquad j,k=1,\ldots,K. \tag{19}$$

Here, V_j^e is the jth port voltage source (usually set equal to 1) of internal impedance Z_0, and $I_{k,j}$ is the resulting current at the kth port when the jth port is excited (the rest of the ports are loaded with Z_0). The right-hand side of (1) corresponding to V_j^e is $\boldsymbol{b}_j$.

If the structure consists of thin wires discretized into segments,[5] the currents $I_{k,j}$ are the elements of the solution vector $\bar{\boldsymbol{x}}_j$ obtained with $\boldsymbol{b}=\boldsymbol{b}_j$. Then, each partial derivative

$$\frac{\partial S_{kj}}{\partial I_{k,j}}=-\frac{2Z_0}{V_j^e},\qquad j,k=1,\ldots,K \tag{20}$$

gives the only nonzero element of the respective adjoint excitation vector $\hat{\boldsymbol{b}}_{kj}$. Its position corresponds exactly to the position of the only nonzero element V_k^e of the original excitation at the kth port $\boldsymbol{b}_k$. This is because $I_{k,j}$ is computed at the very same segment where V_k^e is applied when the kth port is excited. Thus,

$$\hat{\boldsymbol{b}}_{kj}=-\frac{2Z_0}{V_k^e V_j^e}\boldsymbol{b}_k,\qquad j,k=1,\ldots,K. \tag{21}$$

[5]FEKO is primarily an antenna CAD software. It uses the electric-field integral equation (EFIE) for metallic objects and the EFIE with specialized Green's functions for planar layered (printed) circuits. For dielectric objects, it uses a coupled field integral equation (PMCHW) technique. It also employs a fast multipole method (MLFMM) for large problems. The latter does not support specialized Green's functions.

If the structure and, in particular, its ports involve planar or curved metallic surfaces, FEKO applies triangular surface elements accordingly and computes the surface current distribution [19]. In this case, each of the port currents is obtained from the current densities at the edge of its port

$$I_{k,j}=\sum_{i\in\mathcal{S}_k}J_{k,j}^i\Delta l_k^i,\qquad j,k=1,\ldots,K \tag{22}$$

where k denotes the port where the current is computed, and j denotes the port being excited. $J_{k,j}^i$ is the component of the surface current density normal to the edge of the ith element of port k whose length is Δl_k^i. The current densities $J_{k,j}^i, i\in\mathcal{S}_k$, are elements of the solution vector $\boldsymbol{x}_j$, and $\mathcal{S}_k$ is the set of their indices.

We compute the elements of the adjoint excitation vector $\hat{\boldsymbol{b}}_{kj}$ as the derivatives of S_{kj} with respect to $J_{k,j}^i, i\in\mathcal{S}_k$ as follows:

$$[\hat{b}_{kj}]_i=\frac{\partial S_{kj}}{\partial J_{k,i}^{(j)}}=-\frac{2Z_0}{V_e^{(j)}}\cdot\Delta l_{k,i},\qquad i\in\mathcal{S}_k. \tag{23}$$

All elements, for which $i\notin\mathcal{S}_k$, are zero.

On the other hand, the excitation vector $\boldsymbol{b}_k$, corresponding to the kth port excitation of the original problem, also has nonzero elements, whose indices are those in $\mathcal{S}_k$. Moreover, to ensure uniform excitation across the port, these excitation elements are equal to the applied excitation voltage V_k^e, scaled by the edge element Δl_k^i [20] as

$$[b_k]_i=V_k^e\cdot\Delta l_k^i,\qquad i\in\mathcal{S}_k. \tag{24}$$

Comparing (23) and (24), we conclude that the adjoint vectors $\hat{\boldsymbol{b}}_{kj}$ relate to the original excitation $\boldsymbol{b}^{(k)}$ as in (21).

If the MoM matrix fulfills the symmetry condition $\boldsymbol{A}=\boldsymbol{A}^T$, then the adjoint solution vectors $\hat{\boldsymbol{x}}_{kj},\ j,k=1,\ldots,K$ obtained from the adjoint excitations $\hat{\boldsymbol{b}}_{kj}$ relate to the original solution vectors $\boldsymbol{x}_k,\ k=1,\ldots,K$ as[6]

$$\hat{\boldsymbol{x}}_{kj}=\kappa_{kj}\cdot\boldsymbol{x}_k,\kappa_{kj}=-\frac{2Z_0}{V_e^{(k)}V_e^{(j)}}. \tag{25}$$

Thus, with the MoM, we have arrived at a self-adjoint relation similar to the case of the FEM field solution (18).

However, the matrices arising in the large variety of MoM techniques are not always symmetric when a nonuniform unstructured mesh is used, which is usually the case. It would seem that, in the case of an asymmetric MoM matrix, the solution of the adjoint problem is unavoidable. On the other hand, a linear EM problem is intrinsically reciprocal, and, in the limit of an infinitely fine mesh, most MoM techniques tend to produce nearly symmetrical system matrices. In Section VI, we show an important result: if the mesh is suficiently fine to achieve a solution convergence error below 10%, then the asymmetry of the system matrix is negligibly small as far as the sensitivity calculation is concerned. Consequently, the self-adjoint sensitivity analysis using (25) is adequate with a convergent MoM solution. Its sensitivities are practically indistinguishable from those produced by solving the adjoint problem.

[6]A similar relation also exists if $\boldsymbol{A}$ is a Hermitian matrix: $\boldsymbol{A}=\boldsymbol{A}^H=(\boldsymbol{A}^T)^*$.

C. S-Parameter Sensitivity Expression for Linear Systems

To summarize the above theory, we state the sensitivity formula for the self-adjoint S-parameter problem

$$\nabla_{\boldsymbol{p}} S_{kj} = -\kappa_{kj} (\bar{\boldsymbol{x}}_k)^T \cdot \nabla_{\boldsymbol{p}} (A \bar{\boldsymbol{x}}_j), \qquad j,k = 1,\ldots,K. \quad (26)$$

Here, κ_{kj} is a constant, which depends on the powers incident upon the jth and kth ports, as per (18) and (25).

IV. Self-Adjoint Sensitivities of Other Network Parameters

The S-parameters relate to all other types of network parameters through known analytical formulas [21]. Thus, the S-parameter sensitivities can be converted to any other type of network-parameter sensitivities using chain differentiation.

On the other hand, the MoM is well suited for the computation of the input impedance Z_{in} of one-port structures, e.g., antennas. Input-impedance sensitivities have been already considered in [10], [15], and [16]. There, the self-adjoint nature of the problem has not been recognized. As a result, the implementation uses in-house MoM codes, which are modified to carry out the adjoint-problem solution.

Below, we give the coefficient κ in the self-adjoint sensitivity expression for Z_{in} computed with the MoM.

Making use of the MoM port representation explained previously, the relation between the adjoint and the original excitation vectors is obtained as

$$\hat{\boldsymbol{b}} = -I_{\text{in}}^{-2} \cdot \boldsymbol{b} \quad (27)$$

regardless of whether the port consists of a single or multiple wire segments or metallic triangles. Thus, the self-adjoint sensitivity formula for Z_{in} is the same as (26) after replacing S_{kj} with Z_{in} and κ_{kj} with $-I_{\text{in}}^{-2}$. Here, I_{in} is the *complex* current at the port known already from the system analysis.

V. General Procedure and Software Requirements

Assume that the basic steps in the EM structure analysis have already been carried out. These include: 1) a geometrical model of the structure has been built through the graphic user interface of the simulator; 2) a mesh has been generated; 3) the system matrix $\boldsymbol{A}$ has been assembled; and 4) the system equations have been solved for all K port excitations, and the original solution vectors $\bar{\boldsymbol{x}}_k, k = 1,\ldots,K$, of the nominal structure have been found with sufficient accuracy. The self-adjoint sensitivity analysis is then carried out with the following steps.

Step 1) *Parameterization*: Identify design parameters $p_i, i = 1,\ldots,N$.

Step 2) *Generation of Matrix Derivatives*:[7] For each p_i, perturb the structure slightly (with about 1% of the nominal p_i value) while keeping the other parameters at their nominal values. Re-generate the system matrix $\boldsymbol{A}_i = \boldsymbol{A}(\boldsymbol{p} + \Delta p_i \cdot \boldsymbol{u}^i)$, where $\boldsymbol{u}^i$ is a $N \times 1$ vector whose elements are all zero except the ith one, $u_i = 1$. Compute the N derivatives of the system matrix via finite differences

$$\frac{\partial \boldsymbol{A}}{\partial p_i} \approx \frac{\Delta \boldsymbol{A}}{\Delta p_i} = \frac{\boldsymbol{A}_i - \boldsymbol{A}}{\Delta p_i}, \qquad i = 1,\ldots,N. \quad (28)$$

Note that (28) is applicable only if $\boldsymbol{A}$ and $\boldsymbol{A}_i$ are of the same size, i.e., the two respective meshes contain the same number of nodes and elements. Moreover, the numbering of the nodes and elements must correspond to the same locations (within the prescribed perturbation) in the original and perturbed structures, i.e., the mesh topology must be preserved.

Step 3) *Sensitivity Computations*: Use (26) with the proper constant κ.

The above steps show that the EM simulator must have certain features, which enable the self-adjoint sensitivity analysis. First, it must be able to export the system matrix so that the user can compute the system matrix derivatives with (28). Second, it must allow some control over the mesh generation, so that (28) is physically meaningful. Third, it must export the field/current solution vector $\bar{\boldsymbol{x}}$ so that we can compute the sensitivities with (26). The second and third features are available with practically all commercial EM simulators. The first feature deserves more attention. The system matrix is typically very large. In the FEM, it is sparse and can be compressed and further stored in the computer RAM or in a disk file without excessive time delay. In the MoM, however, the matrix is dense, and writing to the disk may be time consuming. Also, only a few of the commercial simulators give access to the generated system matrices. This is why our numerical experiments are carried out with FEKO [19] and with FEMLAB [22]. The first solver, which is based on the MoM, has the option to export the system matrix to a file stored on the disk. It also exports the solution vector with the computed current distribution. FEMLAB is based on the FEM and supports all of these features. Moreover, we can access its system and solution matrices directly without the need to write to the disk.

VI. Validation

We compute the network-parameter sensitivities with our self-adjoint formula and compare the results with those obtained by a forward finite-difference approximation applied directly at the level of the response. This second approach requires a full-wave simulation for each designable parameter. In all plots, our results are marked with SASA (for self-adjoint sensitivity analysis), while the results obtained through direct finite differencing are marked with FD.

A. Sensitivity Solutions With FEM (FEMLAB)

Here, we present two of our validation examples [23]: an H-plane waveguide bend and a dielectric resonator filter [24], both analyzed in their dominant TE_{10} mode. Their H-plane views are shown in Fig. 1. The only design parameter in the waveguide-bend example is the miter length d (the angle is fixed at 45°). We compute the S-parameter derivatives with respect to d in a frequency band from 5.16 to 7.74 GHz (15 frequency

[7]The described procedure uses forward finite differences to obtain the system matrix derivatives. In optimization, a more computationally efficient approach would be the Broyden update [15], [16].

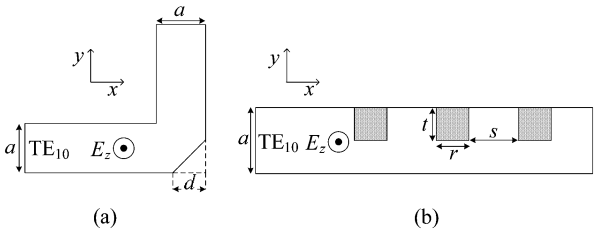

Fig. 1. Top view of the waveguide structures used to validate the sensitivity analysis with the FEM. The waveguide (WR-137) cross section is the same in both examples, $a \times b = 3.48 \times 1.6$ cm. (a) H-plane bend where d is the design parameter, $\boldsymbol{p} = [d]$. (b) Dielectric-resonator filter with three identical dielectric posts ($\varepsilon_r = 38.5, \tan\delta = 2 \times 10^{-4}$), $\boldsymbol{p} = [r/a \;\; s/\lambda_g \; t/a]^T$.

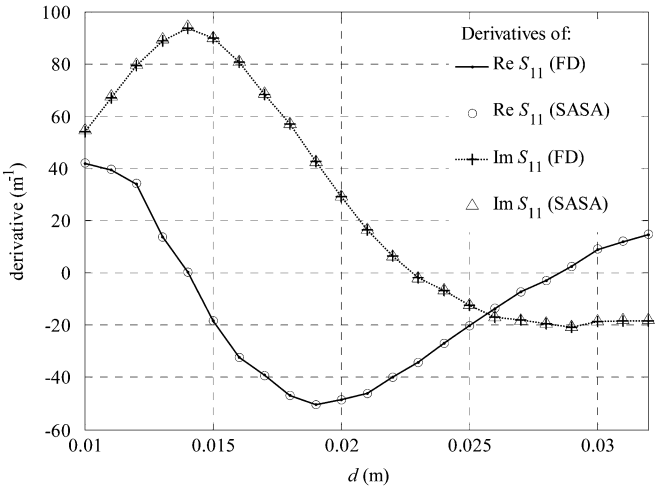

Fig. 2. Derivatives of ReS_{11} and ImS_{11} with respect to d in the waveguide-bend example at $f = 7.74$ GHz.

points). The range of parameter values is $1 \leq d \leq 3.2$ cm with steps of 1 mm. Fig. 2 shows the derivatives of the real and imaginary parts of S_{11} with respect to d at 7.74 GHz. Fig. 3 shows the derivatives of S_{21} at the same frequency. The perturbation of d used in the computation of the system matrix derivative is 1%. The same perturbation is used in the FD computations as well. The agreement between the two sets of data plotted in Figs. 2 and 3 is excellent. This is true for the whole frequency band of interest.

The dielectric-resonator filter [24] is built from three identical rectangular ceramic posts. The material of the posts has complex permittivity $\tilde{\varepsilon} = \varepsilon_0 38.5(1 - j2 \times 10^{-4})$, where ε_0 is the permittivity of vacuum. The design parameters are: the width of the posts normalized to the waveguide width r/a, the distance between the posts normalized with respect to the guided wavelength s/λ_g, and the length of the posts normalized with respect to the waveguide width t/a. Figs. 4–6 show the derivatives of $|S_{11}|$ and $|S_{21}|$ with respect to r/a, s/λ_g and t/a, respectively.[8] The results are for a frequency $f = 6.88$ GHz. Again, very good agreement is observed between the self-adjoint derivatives and the respective finite-difference estimates.

[8]The derivative of the magnitude $|F|$ of a complex response $F = F_R + jF_I$ is obtained from the derivatives of its real and imaginary parts $\frac{\partial |F|}{\partial p} = |F|^{-1} \cdot \left(F_R \frac{\partial F_R}{\partial p} + F_I \frac{\partial F_I}{\partial p}\right)$.

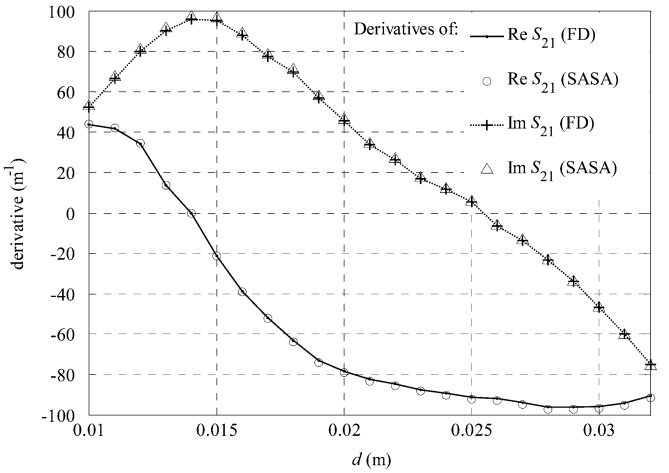

Fig. 3. Derivatives of ReS_{21} and ImS_{21} with respect to d in the waveguide-bend example at $f = 7.74$ GHz.

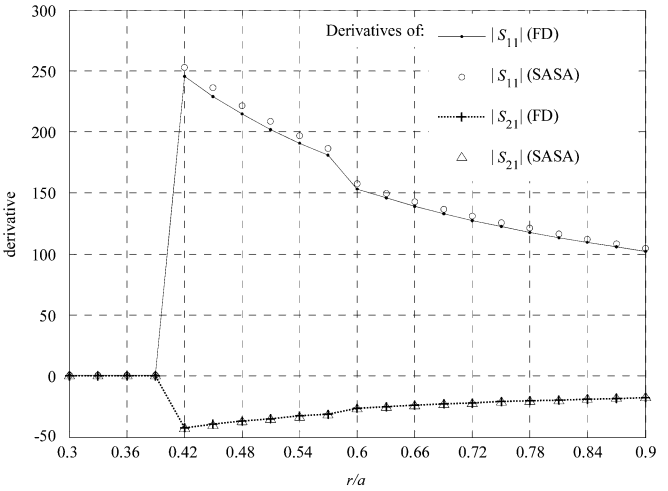

Fig. 4. Derivatives of $|S_{11}|$ and $|S_{21}|$ at 6.88 GHz for the dielectric-resonator filter with respect to r/a. The other design parameters are fixed at $t/a = 0.2, s/\lambda_g = 0.32$.

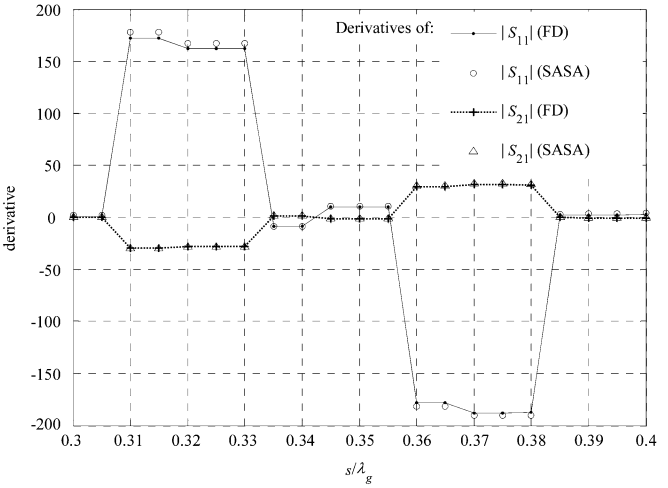

Fig. 5. Derivatives of $|S_{11}|$ and $|S_{21}|$ at 6.88 GHz for the dielectric-resonator filter with respect to s/λ_g. The other design parameters are fixed at $r/a = 0.06, t/a = 0.2$.

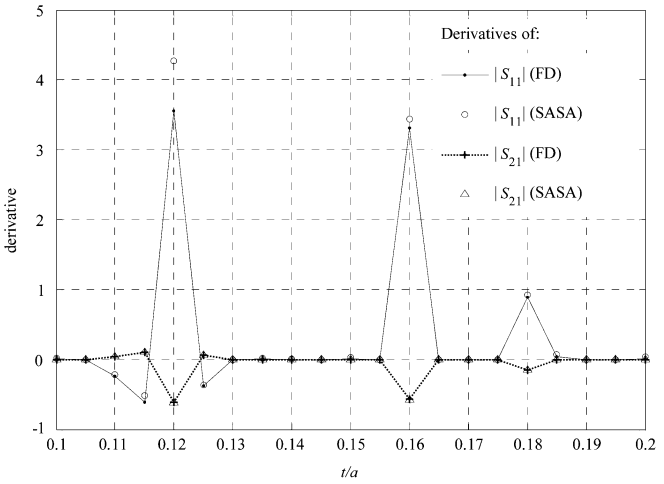

Fig. 6. Derivatives of $|S_{11}|$ and $|S_{21}|$ at 6.88 GHz for the dielectric-resonator filter with respect to t/a. The other design parameters are fixed at $r/a = 0.06, s/\lambda_g = 0.32$.

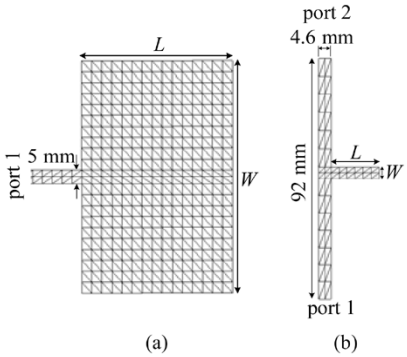

Fig. 7. Top view of the printed structures used to validate the sensitivity analysis with the MoM. (a) Microstrip-fed patch antenna with design parameters $\boldsymbol{p} = [L\ W]^T$. (b) Microstrip bandstop filter with design parameters $\boldsymbol{p} = [L\ W]^T$. The views show the actual mesh.

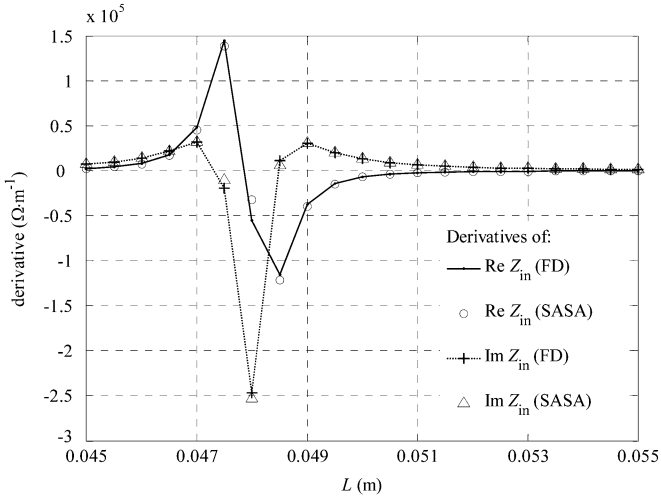

Fig. 8. Derivatives of Z_{in} with respect to the length L of the patch antenna at $f = 2.0$ GHz. Width is at $W = 85$ mm.

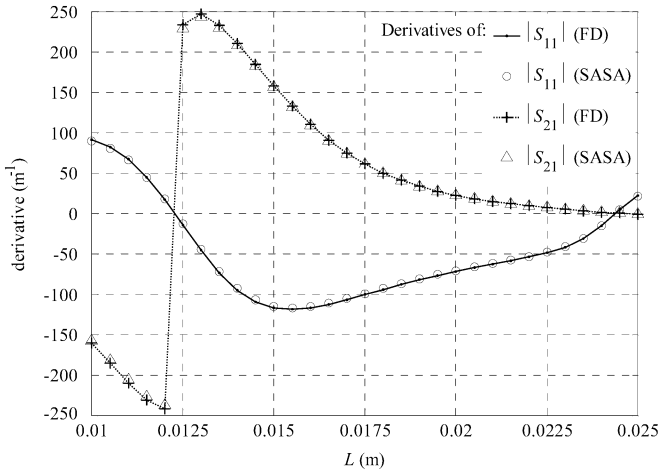

Fig. 9. Derivatives of the S-parameter magnitudes of the bandstop filter with respect to the stub length L at $f = 4.0$ GHz. Width is $W = 4.6$ mm.

B. Sensitivity Solutions With MoM (FEKO)

The calculations of the sensitivities of the S-parameters and the input impedance are validated through a number of FEKO analyses [20], two of which are described next (see Fig. 7). As before, our self-adjoint results are compared with the response derivatives obtained with the finite-difference approximation, which uses 1% parameter perturbation.

1) Input Impedance Sensitivities of a Microstrip-Fed Patch Antenna: The microstrip-fed patch antenna [15] is printed on a substrate of relative dielectric constant $\varepsilon_r = 2.32$ and height $h = 1.59$ mm. The design parameters are its width W and length L shown in Fig. 7(a). The figure shows also the mesh of the metal layer. We compute the sensitivities of the antenna input impedance Z_{in}. Our derivatives with respect to the antenna length L ($45 \leq L \leq 55$ mm) for a width $W = 85$ mm and a frequency of 2.0 GHz are plotted together with the finite-difference results in Fig. 8.

2) S-Parameter Sensitivities of the Bandstop Filter: This simple microstrip filter [see Fig. 7(b)] is printed on a substrate of $\varepsilon_r = 2.33$ and $h = 1.57$ mm. It is analyzed at $f = 4.0$ GHz. The design parameters are the width W and length L of the open-end stub. We compute the sensitivities of the S-parameter magnitudes and phases.[9] Fig. 9 shows the derivatives of $|S_{11}|$ and $|S_{21}|$ with respect to the stub length L when $W = 4.6$ mm. Fig. 10 shows the derivatives of the respective phases.

The self-adjoint sensitivities calculated with the MoM solver disregard the asymmetry of the system matrix as discussed in Section III-B. In Table I, we give quantitative assessment of this asymmetry in the two examples considered above in terms of three measures.

1) Maximum measure:

$$a_{\max} = \max_{\substack{1\leq i\leq M\\ 1\leq j\leq M}} \left| \frac{A_{ij} - A_{ji}}{A_{ij}} \right|. \tag{29}$$

2) ℓ_1 measure:

$$a_{\ell 1} = \frac{2}{M^2} \sum_{i=1}^{M-1} \sum_{j=i+1}^{M} \left| \frac{A_{ij} - A_{ji}}{A_{ij}} \right|. \tag{30}$$

[9]The derivative of the phase ϕ of a complex response $|F|e^{j\phi} = F_R + jF_I$ is obtained from the derivatives of its real and imaginary parts $\frac{\partial \phi}{\partial p} = |F|^{-2} \cdot \left(F_R \frac{\partial F_I}{\partial p} - F_I \frac{\partial F_R}{\partial p} \right)$.

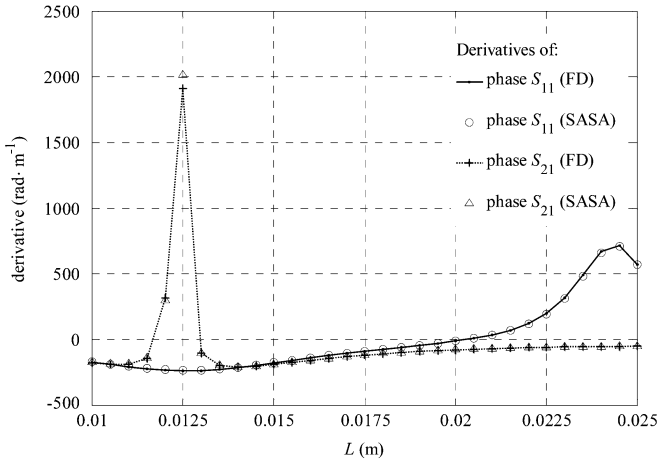

Fig. 10. Derivatives of the S-parameter phases of the bandstop filter with respect to the stub length L at $f = 4.0$ GHz. Width is $W = 4.6$ mm.

TABLE I
ASYMMETRY MEASURES OF MoM MATRICES IN VALIDATION EXAMPLES

	patch antenna	bandstop filter
asymmetry measure $a_{\max}$	263	10.38
asymmetry measure $a_{\ell 1}$	0.3287	0.2333
asymmetry measure $a_{\ell 2}$	0.0012	0.0194

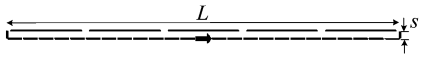

Fig. 11. Folded dipole and one of its coarse nonuniform segmentations in FEKO (32 segments). The radius of the wire is $a = 10^{-4}\lambda$ and the spacing between the wires is $s = 10^{-3}\lambda$. L is a design parameter, $0.2\lambda \leq L \leq 1.2\lambda$. The arrow in the center of the lower wire indicates the feed point.

3) ℓ_2 measure:

$$a_{\ell 2} = \frac{1}{M^2}\sqrt{2\sum_{i=1}^{M-1}\sum_{j=i+1}^{M}\left|\frac{A_{ij}-A_{ji}}{A_{ij}}\right|^2}. \tag{31}$$

The excellent agreement between the self-adjoint sensitivities and the finite-difference sensitivities shown in Figs. 8–10 asserts that the asymmetry measures summarized in Table I are minor as far as the sensitivity calculations are concerned. We need, however, a robust criterion, which can assure the accuracy of the sensitivity result without the need to check against a reference.

3) MoM Matrix Symmetry Versus Convergence of Solution: We carry out the following experiment. We analyze the folded dipole shown in Fig. 11. The radius of the wire is $a = 10^{-4}\lambda$ and the spacing between the two wires is $s = 10^{-3}\lambda$. The length L varies from 0.2λ to 1.2λ. The response is the antenna input impedance Z_{in}. We force the maximum segment size on one of the two parallel wires to be five times larger than that on the other wire. This leads to very different segment lengths along the two parallel wires (see Fig. 11). Since the two wires are very close, the MoM matrix is quite asymmetric. We emphasize that this is an abnormal (not recommended) segmentation allowing us to investigate a worst case scenario. Normally, the user sets a global maximum segment length, which is applied to the entire structure, with the result being a relatively uniform segmentation or mesh.

TABLE II
CONVERGENCE ERROR AND MATRIX ASYMMETRY MEASURES IN THE MESH REFINEMENT FOR THE FOLDED DIPOLE

iteration	1	2	3	4	5	6
segments	32	68	140	272	548	1088
E, %	NA	25.99	9.665	1.918	1.097	0.8928
$a_{\ell 2}$	66.03	88.21	11.72	1.435	0.1101	0.0074
$a_{\ell 1}$	286.8	421.0	86.16	16.32	2.347	0.4261
$a_{\max}$	19887	91119	34588	11274	2425	1682

We next perform mesh refinement starting from a coarse mesh of 32 segments. Each iteration of the mesh refinement involves: 1) a decrease of the mesh elements by a certain factor and 2) full-wave analysis with the current mesh. We decrease the maximum element size by approximately 50% for each of the two parallel wires of the folded dipole. The ratio of 5 between them is preserved. The mesh refinement continues until a convergence error less than 1% is achieved. The convergence error at the kth iteration is defined as

$$E^{(k)} = \frac{\left|Z_{\text{in}}^{(k)} - Z_{\text{in}}^{(k-1)}\right|}{\left|Z_{\text{in}}^{(k)}\right|}\cdot 100\%. \tag{32}$$

Here, $Z_{\text{in}}^{(k)}$ and $Z_{\text{in}}^{(k-1)}$ are the complex input impedances computed at the kth and $(k-1)$th analyses. Convergence is achieved with a mesh of 1088 segments.

At each of the above analyses, we compute the matrix asymmetry measures, which are summarized in Table II. We see that, as soon as convergence is achieved, the asymmetry measures $a_{\ell 2}$ and $a_{\ell 1}$ become comparable to those in the validation examples (see Table I).

At every iteration of the mesh refinement, we also compute the derivative $\partial Z_{\text{in}}/\partial L$ (at $L = 0.5\lambda$) with our self-adjoint approach, i.e., ignoring the system matrix asymmetry. We compare the self-adjoint result for each mesh with its respective reference sensitivity. The reference sensitivity is computed with our original adjoint technique [10], which solves the adjoint problem (4), i.e., it fully accounts for the asymmetry of the system matrix.[10] We define the asymmetry error in the computed response derivative D as

$$e_D = \frac{|D-\bar{D}|}{|\bar{D}|}\cdot 100\% \tag{33}$$

where $\bar{D}$ is the reference derivative.

In Fig. 12, we plot the asymmetry derivative error e_D for $\partial Z_{\text{in}}/\partial L$ and the matrix asymmetry measure $a_{\ell 2}$ versus the convergence error E of the MoM solution [see (32)]. First, we see that $a_{\ell 2}$ increases as the convergence error E increases with a slope, which is very similar to that of e_D (unlike $a_{\ell 1}$ and $a_{\max}$). Apparently, $a_{\ell 2}$ is the matrix asymmetry measure, which can serve as a criterion for an accurate self-adjoint sensitivity calculation. As long as its value is below 2%, we can expect e_D

[10]We note that FEKO exports not only the MoM system matrix but also its $\boldsymbol{L}$ and $\boldsymbol{U}$ factors. Thus, the adjoint problem solution is very fast [10].

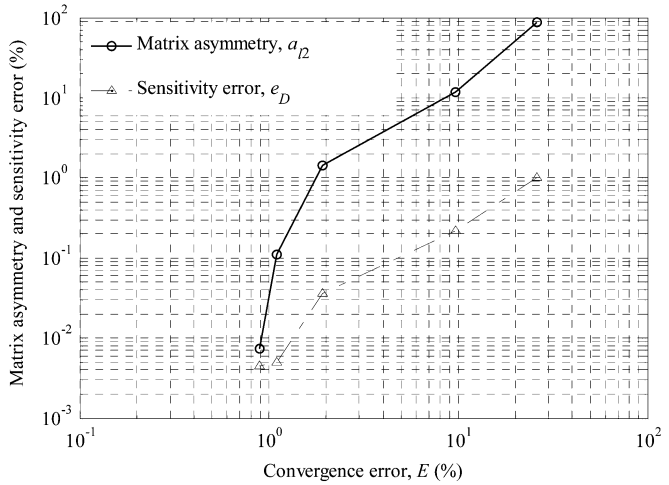

Fig. 12. Matrix asymmetry measure and the error of the computed derivative $\partial Z_{\rm in}/\partial L$ (at $L = 0.5\lambda$) as a function of the convergence error of the analysis in the folded-dipole example.

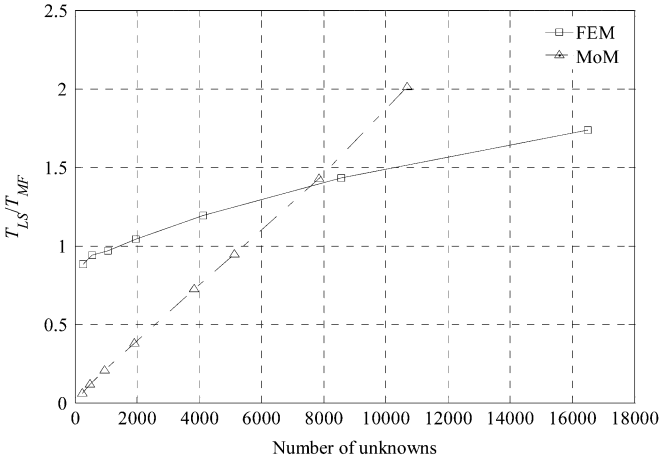

Fig. 13. Ratio between the time required to solve the linear system and the time required to assemble the system matrix in FEMLAB (FEM) and FEKO (MoM).

to be well below 1%. Second, we conclude that as soon as an acceptable convergence is achieved in the response calculation ($E \leq 10\%$), we can have full confidence in the self-adjoint response sensitivity calculation since its asymmetry error e_D is well below E, typically by two orders of magnitude.

In summary, if the MoM solution is set up properly and it yields network parameters of acceptable accuracy,[11] it can be used to compute accurate network-parameter sensitivities with the self-adjoint approach. This approach is robust and insensitive to the asymmetry of the MoM system matrix.

For completeness, we note that our methodology is applicable when the MoM matrix is fully computed and is made accessible. The nature of the linear-system solver (direct or iterative) is unimportant in the self-adjoint analysis since an adjoint solution is not needed. However, MoM techniques based on fast multipole expansions do not compute the full matrix and are thus not well suited for adjoint-based sensitivity analysis. For them, specialized adjoint-based algorithms need to be developed and, at this stage, applications with commercial solvers do not seem feasible. Response sensitivities with finite differences, however, are an option.

VII. Computational Overhead of the Self-Adjoint Sensitivity Analysis

A. CPU Time Overhead

The computational overhead associated with the self-adjoint sensitivity analysis is due to two types of calculations: 1) the system matrix derivatives, $\partial \boldsymbol{A}/\partial p_i, i = 1, \ldots, N$, and 2) the row-matrix-column multiplications involved in the sensitivity formula (26). Compared to the full-wave analysis, the sensitivity formula (26) requires insignificant CPU time, which is often neglected. We denote the time required to compute one derivative with the sensitivity formula as $T_{\rm SF}$. In comparison, the calculation of the N system matrix derivatives is much more time consuming. Whether it employs finite differences or analytical expressions, it is roughly equivalent to N matrix fills.[12] A matrix fill, especially in the MoM, can be time-consuming. We denote the time for one matrix fill as $T_{\rm MF}$. Thus, the overhead time required by the self-adjoint sensitivity analysis is

$$T_{\rm SASA} = N \cdot T_{\rm MF} + N \cdot T_{\rm SF}. \tag{34}$$

On the other hand, if we employ forward finite differences directly at the level of the response in order to compute the N derivatives of the network parameters, we need N additional full analyses, each involving a matrix fill and a linear system solution. Thus, the overhead of the finite-difference sensitivity analysis is

$$T_{\rm FD} = N \cdot T_{\rm MF} + N \cdot T_{\rm LS} \tag{35}$$

where $T_{\rm LS}$ is the time required to solve (1).

We can define a time-saving factor as the ratio $S_T = T_{\rm FD}/T_{\rm SASA}$, which is a measure of the CPU savings offered by our sensitivity analysis approach

$$S_T = \frac{T_{\rm MF} + T_{\rm LS}}{T_{\rm MF} + T_{\rm SF}}. \tag{36}$$

Since $T_{\rm SF}$ is negligible in comparison with $T_{\rm MF}$, we have

$$S_T \approx 1 + \frac{T_{\rm LS}}{T_{\rm MF}}. \tag{37}$$

Evidently, the larger the ratio $R = T_{\rm LS}/T_{\rm MF}$ is, the larger our time savings are. Notice that $S_T \geq 1$, i.e., our approach would never perform worse than the finite-difference approach. R depends on the size of the problem—it grows as the number of unknowns M increases. This dependence is stronger in the MoM.

Fig. 13 shows the ratios $R = T_{\rm LS}/T_{\rm MF}$ of the FEKO and FEMLAB solvers. The FEKO data are generated with a seven-element Yagi–Uda antenna [10], [25] analyzed with increasingly finer segmentations whereby the number of unknowns increases from 240 to 11 220. The FEMLAB data are generated with a dielectric-slab waveguide filter [26], [27] where we increase the number of unknowns from 254 to 16 495 through

[11]Convergence analysis is desirable in order to verify that the solution accuracy is "acceptable." Most commercial MoM solvers do not perform automated mesh refinement but manual refinement is always possible.

[12]If the Broyden update is used to compute the system matrix derivatives, this overhead is negligible [15], [16].

TABLE III
FEMLAB COMPUTATIONAL OVERHEAD OF SENSITIVITY ANALYSIS WITH THE SELF-ADJOINT METHOD AND WITH THE FINITE DIFFERENCES ($N = 1$)

M	254	555	1060	1951	4129	8557	16495
T_{SASA} (s)	17.4	17.9	18.2	19.4	21.1	25.1.8	32.4
T_{FD} (s)	18.2	19.3	20.9	23.7	31.1	47.3	81.8
S_T	1.04	1.08	1.15	1.21	1.47	1.88	2.52

TABLE IV
FEKO COMPUTATIONAL OVERHEAD OF SENSITIVITY ANALYSIS WITH THE SELF-ADJOINT METHOD AND WITH THE FINITE DIFFERENCES ($N = 1$)

M	240	480	960	1920	3840	7860	10680
T_{SASA} (s)	0.265	0.922	3.469	13.797	53.593	209.7	398.3
T_{FD} (s)	0.281	1.032	4.187	19.031	92.374	509.2	1188
S_T	1.060	1.119	1.207	1.379	1.724	2.429	2.983

TABLE V
FEMLAB COMPUTATIONAL OVERHEAD OF SENSITIVITY ANALYSIS WITH THE SELF-ADJOINT METHOD AND WITH THE FINITE DIFFERENCES ($M = 50\,000$)

N	1	2	3	4	5	6	7
T_{SASA} (s)	32.6	66.0	99.0	135.0	167.0	200.2	236.2
T_{FD} (s)	129.1	261.0	394.6	521.6	646.1	790.0	919.5
S_T	3.96	3.95	3.99	3.86	3.87	3.95	3.89

TABLE VI
FEKO COMPUTATIONAL OVERHEAD OF SENSITIVITY ANALYSIS WITH THE SELF-ADJOINT METHOD AND WITH THE FINITE DIFFERENCES ($M = 10\,680$)

N	1	3	5	7	9	11
T_{SASA} (s)	398.34	1193.7	1988.0	2782.3	3576.4	4371.3
T_{FD} (s)	1188.3	3560.0	5925.8	8292.1	10660	13024
S_T	2.9831	2.9823	2.9808	2.9803	2.9807	2.9794

mesh refinement. The plotted ratios are only representative since they depend on the type of the mesh (segments or triangles in FEKO) and on the type of the linear-system solver (direct or iterative). The trend of the ratio increasing with the size of the problem is general. We also emphasize that we record the CPU time only. With large matrices, a computer may run out of memory (RAM), in which case, part of the data is swapped to the disk. This causes a significant increase of $T_{\rm LS}$ and R, which is machine and hard-drive dependent. This is not taken into account.

In Table III, we show the actual CPU time spent for response sensitivity calculations with our self-adjoint approach and the finite-difference approximation using the FEMLAB solver. Table IV shows the same information for the FEKO analysis. We consider the case of one design parameter ($N = 1$), i.e., a single derivative is computed. The size of the system M varies. The increase of the time-saving factor S_T as the number of unknowns increases corresponds closely to the ratio curves $R = T_{\rm LS}/T_{\rm MF}$ plotted in Fig. 13 in accordance with (37). The analyzed structures are the same as those used to investigate the $T_{\rm LS}/T_{\rm MF}$ ratios.

We also carry out a time comparison between our approach and the finite-difference approach when the size of the system M is fixed, but the number of design parameters N varies. The FEM and MoM results are summarized in Tables V and VI, respectively. As predicted by (37), the time savings are practically independent of the number of design parameters.

B. Possible Further Reduction of Overhead

We reiterate that, in optimization, the Broyden update is a far more efficient alternative to the computation of the system matrix derivatives [15], [16]. With it, S_T becomes roughly proportional to $(T_{\rm MF} + T_{\rm LS})/T_{\rm SF}$, which is normally a very large ratio. The application of this algorithm in optimization is to be discussed elsewhere.

It is important to understand that in our implementation we do not have access to the meshing and matrix-assembly modules of the EM simulators. As a result, full re-meshing and a matrix fill are required to obtain the system matrix derivative for each of the N design parameters. If the self-adjoint algorithm is to be implemented *within* an EM solver, which already has parameterization available, the time required for a perturbed-geometry matrix fill $T_{\rm MF}$ may be drastically reduced [10]. This is because the parameterization necessarily flags all mesh elements affected by a parameter perturbation. It is then a relatively simple task to link the affected mesh elements to the affected matrix elements, and recompute only the affected elements instead of recomputing the whole system matrix. The number of affected matrix elements is very small and the system matrix derivative is very sparse when a shape parameter is perturbed. When global material parameters are perturbed, many or all of the matrix elements change, and the system matrix derivative [12] is dense.

VIII. CONCLUSION

We have proposed an adjoint-variable approach to the computation of the network-parameter sensitivities, which is independent of the EM analysis engine. It exploits the self-adjoint nature of the sensitivity problem in a linear medium thereby replacing the adjoint-variable solution with the properly scaled solution of the original problem. Not only does this reduce the computational overhead of the sensitivity computation but it significantly simplifies the implementation by making it completely independent of the EM analysis code. We discuss the implementation with particular commercial MoM and FEM EM solvers, which support the features enabling the sensitivity analysis. Our methodology, however, is general, and with the proper choice of the complex constant relating the adjoint and original solutions, it can be applied to other FEM or MoM simulators.

We provide thorough investigation of the accuracy and the CPU time requirements of the self-adjoint algorithm. We show that the CPU time overhead of the sensitivity analysis can be significantly reduced by using our adjoint technique as compared to the direct finite differences at the response level. The larger the size of the problem is, the larger the time savings factor is.

ACKNOWLEDGMENT

The authors would like to thank Dr. C. J. Reddy, EM Software & Systems USA, Hampton, VA, and the team at FEKO Technical Support, Hampton, VA, for their patience and help regarding the technical details in handling the exported data from the FEKO simulator.

REFERENCES

[1] D. G. Cacuci, *Sensitivity & Uncertainty Analysis, Volume 1: Theory*. Boca Raton, FL: Chapman & Hall/CRC, 2003.

[2] A. D. Belegundu and T. R. Chandrupatla, *Optimization Concepts and Applications in Engineering*. Upper Saddle River, NJ: Prentice-Hall, 1999.

[3] E. J. Haug, K. K. Choi, and V. Komkov, *Design Sensitivity Analysis of Structural Systems*. Orlando, FL: Academic, 1986.

[4] P. Neittaanmäki, M. Rudnicki, and A. Savini, *Inverse Problems and Optimal Design in Electricity and Magnetism*. New York: Oxford Univ. Press, 1996, ch. 4.

[5] H.-B. Lee and T. Itoh, "A systematic optimum design of waveguide-to-microstrip transition," *IEEE Trans. Microw. Theory Tech.*, vol. 45, no. 5, pp. 803–809, May 1997.

[6] H. Akel and J. P. Webb, "Design sensitivities for scattering-matrix calculation with tetrahedral edge elements," *IEEE Trans. Magn.*, vol. 36, no. 4, pp. 1043–1046, Jul. 2000.

[7] J. P. Webb, "Design sensitivity of frequency response in 3-D finite-element analysis of microwave devices," *IEEE Trans. Magn.*, vol. 38, no. 2, pp. 1109–1112, Mar. 2002.

[8] Y. S. Chung, C. Cheon, I. H. Park, and S. Y. Hahn, "Optimal design method for microwave device using time domain method and design sensitivity analysis—Part I: FETD case," *IEEE Trans. Magn.*, vol. 37, no. 5, pp. 3289–3293, Sep. 2001.

[9] N. K. Nikolova, J. W. Bandler, and M. H. Bakr, "Adjoint techniques for sensitivity analysis in high-frequency structure CAD," *IEEE Trans. Microw. Theory Tech.*, vol. 52, no. 1, pp. 403–419, Jan. 2004.

[10] N. K. Georgieva, S. Glavic, M. H. Bakr, and J. W. Bandler, "Feasible adjoint sensitivity technique for EM design optimization," *IEEE Trans. Microw. Theory Tech.*, vol. 50, no. 12, pp. 2751–2758, Dec. 2002.

[11] S. M. Ali, N. K. Nikolova, and M. H. Bakr, "Recent advances in sensitivity analysis with frequency-domain full-wave EM solvers," *Appl. Comput. Electromagn. Soc. J.*, vol. 19, pp. 147–154, Nov. 2004.

[12] M. H. Bakr and N. K. Nikolova, "An adjoint variable method for frequency domain TLM problems with conducting boundaries," *IEEE Microw. Wireless Compon. Lett.*, vol. 13, no. 9, pp. 408–410, Sep. 2003.

[13] S. M. Ali, N. K. Nikolova, and M. H. Bakr, "Recent advances in sensitivity analysis with frequency-domain full-wave EM solvers," *Appl. Comput. Electromagn. Soc. J.*, vol. 19, pp. 147–154, Nov. 2004.

[14] M. D. Greenberg, *Advanced Engineering Mathematics*. Upper Saddle River, NJ: Prentice-Hall, 1998, pp. 1138–1140.

[15] N. K. Nikolova, R. Safian, E. A. Soliman, M. H. Bakr, and J. W. Bandler, "Accelerated gradient based optimization using adjoint sensitivities," *IEEE Trans. Antennas Propag.*, vol. 52, no. 8, pp. 2147–2157, Aug. 2004.

[16] E. A. Soliman, M. H. Bakr, and N. K. Nikolova, "Accelerated gradient-based optimization of planar circuits," *IEEE Trans. Antennas Propag.*, vol. 53, no. 2, pp. 880–883, Feb. 2005.

[17] J. Jin, *The Finite Element Method in Electromagnetics*, 2nd ed. New York: Wiley, 2002, p. 310, 311, 496, 497.

[18] M. Salazar-Palma, T. K. Sarkar, L.-E. García-Castillo, T. Roy, and A. Djordjević, *Iterative and Self-Adaptive Finite-Elements in Electromagnetic Modeling*. Norwood, MA: Artech, 1998, pp. 465–466.

[19] *FEKO User's Manual, Suite 4.2*, EM Software & Systems (USA), Inc., Hampton, VA, Jun. 2004. [Online]. Available: http://www.feko.info, http://www.emssusa.com/.

[20] "Comput. Electromagn. Res. Lab.," McMaster Univ., Hamilton, ON, Canada, Rep. CEM-R-23, Jun. 2005.

[21] D. M. Pozar, *Microwave Engineering*, 2nd ed. New York: Wiley, 1998, pt. 4.

[22] *User's Guide, FEMLAB 3.1*, COMSOL Inc., Burlington, MA, 2004. [Online]. Available: http://www.comsol.com..

[23] "Comput. Electromagn. Res. Lab.," McMaster Univ., Hamilton, ON, Canada, Rep. CEM-R-21, Jun. 2005.

[24] L. Minakova and L. Rud, "Spectral approach to the synthesis of the waveguide bandstop filters based on dielectric rectangular posts," in *Proc. Int. Math. Methods Electromagn. Theory Conf.*, vol. 2, Sep. 2000, pp. 479–481.

[25] "Comput. Electromagn. Res. Lab.," McMaster Univ., Hamilton, ON, Canada, Rep. CEM-R-24, Jun. 2005.

[26] "Comput. Electromagn. Res. Lab.," McMaster Univ., Hamilton, ON, Canada, Rep. CEM-R-22, Jun. 2005.

[27] A. Abdelmonem, J.-F. Liang, H.-W. Yao, and K. A. Zaki, "Spurious free D.L. TE mode band pass filter," in *IEEE MTT-S Int. Microw. Symp. Dig.*, vol. 2, May 1994, pp. 735–738.

Natalia K. Nikolova (S'93–M'97–SM'05) received the Dipl. Eng. degree from the Technical University of Varna, Varna, Bulgaria, in 1989, and the Ph.D. degree from the University of Electro-Communications, Tokyo, Japan, in 1997.

From 1998 to 1999, she was with the Natural Sciences and Engineering Research Council of Canada (NSERC), during which time she was initially with the Microwave and Electromagnetics Laboratory, DalTech, Dalhousie University, Halifax, NS, Canada, and then for a year with the Simulation Optimization Systems Research Laboratory, McMaster University, Hamilton, ON, Canada. In July 1999, she joined the Department of Electrical and Computer Engineering, McMaster University, where she is currently an Associate Professor. Her research interests include theoretical and computational electromagnetism, high-frequency analysis techniques, as well as computer-aided design (CAD) methods for high-frequency structures and antennas.

Dr. Nikolova is a member of the Applied Computational Electromagnetics Society. She is also an International Union of Radio Science (URSI) correspondent, Commissions B and D, and a representative of Commission D of the URSI Canadian National Committee. She was the recipient of an NSERC Post-Doctoral Fellowship from 1998 to 1999. She held a University Faculty Award of the NSERC from 2000 to 2005.

Jiang Zhu was born in Sichuan, China, in 1980. He received the B.Eng. degree in electrical engineering from Zhejiang University, Hangzhou, China, in 2003, and is currently working toward the M.A.Sc. degree at McMaster University, Hamilton, ON, Canada.

In September 2004, he joined the Computational Electromagnetics Research Laboratory and the Simulation Optimization Systems Research Laboratory, Department of Electrical and Computer Engineering, McMaster University, where he is currently a Research Assistant. His research interests include microwave computer-aided design, EM optimization, modeling of microwave circuits and antennas, and bio-electromagnetics.

Dongying Li received the B.Sc. degree in electrical engineering from Shanghai Jiao Tong University, Shanghai, China, in 2004, and is currently working toward the M.A.Sc. degree in electrical engineering at McMaster University, Hamilton, ON, Canada.

During this time, he has been a Research Assistant with the Computational Electromagnetics Research Laboratory, McMaster University. His research interests include computational electromagnetics, optimization methods, and nondestructive testing methodologies.

Mohamed H. Bakr (S'98–M'00) received the B.Sc. degree in electronics and communications engineering with distinction (honors) and the M.Sc. degree in engineering mathematics from Cairo University, Cairo, Egypt, in 1992 and 1996, respectively, and the Ph.D. degree from McMaster University, Hamilton, ON, Canada, in 2000.

In 1997, he was a student intern with Optimization Systems Associates Inc. (OSA), Dundas, ON, Canada. From 1998 to 2000, he was a Research Assistant with the Simulation Optimization Systems (SOS) Research Laboratory, McMaster University. In November 2000, he joined the Computational Electromagnetics Research Laboratory (CERL), University of Victoria, Victoria, BC, Canada, as a Natural Sciences and Engineering Research Council of Canada (NSERC) Post-Doctoral Fellow. He is currently an Assistant Professor with the Department of Electrical and Computer Engineering, McMaster University. His research areas of interest include optimization methods, computer-aided design and modeling of microwave circuits, neural-network applications, smart analysis of microwave circuits, and efficient optimization using time-/frequency-domain methods.

Dr. Bakr was a recipient of the Premier's Research Excellence Award (PREA) presented by the Province of Ontario, Canada, in 2003.

John W. Bandler (S'66–M'66–SM'74–F'78) was born in Jerusalem on November 9, 1941. He received the B.Sc. (Eng.), Ph.D., and D.Sc. (Eng.) degrees from the University of London, London, U.K., in 1963, 1967, and 1976, respectively.

In 1966, he joined Mullard Research Laboratories, Redhill, Surrey, U.K. From 1967 to 1969, he was a Post-Doctorate Fellow and Sessional Lecturer with the University of Manitoba, Winnipeg, MB, Canada. In 1969, he joined McMaster University, Hamilton, ON, Canada, where he has served as Chairman of the Department of Electrical Engineering and Dean of the Faculty of Engineering. He is currently Professor Emeritus in Electrical and Computer Engineering and directs research in the Simulation Optimization Systems Research Laboratory. He was President of Optimization Systems Associates, Inc. (OSA), Dundas, ON, Canada, which he founded in 1983, until November 20, 1997, the date of acquisition of OSA by the Hewlett-Packard Company (HP). OSA implemented a first-generation yield-driven microwave CAD capability for Raytheon in 1985, followed by further innovations in linear and nonlinear microwave CAD technology for the Raytheon/Texas Instruments Joint Venture MIMIC Program. OSA introduced the computer-aided engineering (CAE) systems RoMPE in 1988, HarPE in 1989, OSA90 and OSA90/hope in 1991, Empipe in 1992, and Empipe3D and EmpipeExpress in 1996. OSA created ***empath*** in 1996, marketed by Sonnet Software, Inc. He is currently President of Bandler Corporation, Dundas, ON, Canada, which he founded in 1997. He has authored or coauthored over 370 papers from 1965 to 2005. He contributed to *Modern Filter Theory and Design* (New York: Wiley-Interscience, 1973) and *Analog Methods for Computer-aided Analysis and Diagnosis* (New York: Marcel Dekker, 1988). Four of his papers have been reprinted in *Computer-Aided Filter Design* (New York: IEEE Press, 1973), one in each of *Microwave Integrated Circuits* (Norwood, MA: Artech House, 1975), *Low-Noise Microwave Transistors and Amplifiers* (New York: IEEE Press, 1981), *Microwave Integrated Circuits, 2nd ed.*(Norwood, MA: Artech House, 1985), *Statistical Design of Integrated Circuits* (New York: IEEE Press, 1987), and *Analog Fault Diagnosis* (New York: IEEE Press, 1987). He joined the Editorial Boards of the *International Journal of Numerical Modeling* (1987), the *International Journal of Microwave and Millimeterwave Computer-Aided Engineering* (1989), and *Optimization Eng.* in 1998. He was Guest Editor of the *International Journal of Microwave and Millimeter-Wave Computer-Aided Engineering* Special Issue on Optimization-Oriented Microwave CAD (1997). He was guest co-editor of the *Optimization and Engineering* Special Issue on Surrogate Modeling and Space Mapping for Engineering Optimization (2001).

Dr. Bandler is a Fellow of the Canadian Academy of Engineering, the Royal Society of Canada, the Institution of Electrical Engineers (U.K.), and the Engineering Institute of Canada. He is a member of the Association of Professional Engineers of the Province of Ontario (Canada) and a member of the Massachusetts Institute of Technology (MIT) Electromagnetics Academy. He was an Associate Editor of the IEEE TRANSACTIONS ON MICROWAVE THEORY AND TECHNIQUES (T-MTT) from 1969 to 1974 and has continued serving as a member of the Editorial Board. He was Guest Editor of the T-MTT Special Issue on Computer-Oriented Microwave Practices (1974) and Guest Coeditor of the IEEE T-MTT Special Issue on Process-Oriented Microwave CAD and Modeling (1992). He was Guest Editor of the IEEE T-MTT Special Issue on Automated Circuit Design Using Electromagnetic Simulators (1997). He was Guest Coeditor of the IEEE T-MTT Special Issue on Electromagnetics-Based Optimization of Microwave Components and Circuits (2004). He has served as chair of the MTT-1 Technical Committee on Computer-Aided Design. He was the recipient of the 1994 Automatic Radio Frequency Techniques Group (ARFTG) Automated Measurements Career Award and the 2004 Microwave Application Award presented by the IEEE MTT-S.